PERGAMON

International Journal of Solids and Structures 40 (2003) 6095–6109

INTERNATIONAL JOURNAL OF SOLIDS and STRUCTURES

www.elsevier.com/locate/ijsolstr

Koiter circles in the buckling of axially compressed conical shells

Andrea Spagnoli *

Department of Civil and Environmental Engineering, & Architecture, University of Parma Parco Area delle Scienze 181/A, 43100 Parma, Italy

Received 14 November 2002

Abstract

As is well known, the elastic stability of shell structures under certain loading conditions is characterised by a severely unstable postbuckling behaviour. The presence of simultaneous buckling modes ('competing' modes corresponding to the same critical buckling load) is deemed to be largely responsible for such a behaviour. In the present paper, within the framework of the so-called classical theory (linear bifurcation eigenvalue analysis), the buckling behaviour of axially compressed cylindrical shells is firstly reviewed. Accordingly, doubly periodic eigenvectors (buckling modes) corresponding to the same eigenvalue (critical buckling load) can be determined, and their locus in a dimensionless meridional and circumferential buckling wavenumber space is described by a circle (known as the *Koiter circle*). In the case of axially compressed conical shells, no clear evidence of the existence of simultaneous buckling modes can be found in the literature. Then, such a problem is studied here via linear eigenvalue finite element analyses, showing that simultaneous doubly periodic modes do also occur for cones, and that their locus in a specifically defined dimensionless wavenumber space can be described by an ellipse (hereafter termed as the *Koiter ellipse*) whose aspect ratio is dependent on the tapering angle of the cone.

Keywords: Buckling; Conical shells; Linear stability; Simultaneous modes

1. Introduction

Buckling is often the main cause of collapse in thin-walled shell structures submitted to compressive stresses. As is well known, even in the case of fully elastic behaviour of the material the actual collapse load might be dramatically lower than the critical buckling (bifurcation) load obtained from linear eigenvalue analysis, due to the presence of unintentional imperfections (geometrical, of loading, etc.). Hence, the evaluation of the actual collapse load is a difficult task involving non-linear analysis. Among the shell stability problems, that of cylinders has thoroughly been studied, because of their simple geometry. In particular, the loading condition of axial compression has largely been investigated due to the related high

* Tel.: +39-0521-905927; fax: +39-0521-905-924.
E-mail address: spagnoli@unipr.it (A. Spagnoli).

0020-7683/$ - see front matter © 2003 Elsevier Ltd. All rights reserved.
doi:10.1016/S0020-7683(03)00369-X

Nomenclature

C	extensional stiffness parameter: $C = Et/\lfloor 12(1-\nu^2)\rfloor$
D	bending stiffness parameter: $D = Et^3/\lfloor 12(1-\nu^2)\rfloor$
E	Young's modulus
$F(\beta_m, \beta_c)$	locus of simultaneous buckling modes in the dimensionless wavenumber space
l_0	meridional half wavelength for axisymmetric buckling of axially compressed cylinders (see Eq. (8))
l_m	meridional buckling half wavelength for cylinders (see Eq. (10a))
$\bar{l}_m$	meridional buckling half wavelength for cones (see Eq. (25a))
l_c	circumferential buckling half wavelength for cylinders (see Eq. (10b))
$\bar{l}_c$	average circumferential buckling half wavelength for cones (see Eq. (25b))
L	slant length of cone
m	number of meridional buckling half waves
n	number of circumferential buckling full waves
P	applied load or buckling load (linear eigenvalue analysis)
P'	dimensionless load parameter (see Eq. (21))
P_{cone}	Seide's buckling load for axially compressed cones (see Eq. (2))
P_{cyl}	classical buckling load for axially compressed cylinders (see Eq. (1))
R	radius of cylinder
$R(x)$	radius of cone at any point
$\overline{R}$	average radius of cone, $\overline{R} = (R_1 + R_2)/2$
s	meridional coordinate measured from the cone apex (see Fig. 1)
s'	dimensionless meridional coordinate, $s' = s/s_2$
t	shell thickness
u	displacement in meridional direction, positive towards the large radius (see Fig. 1)
v	displacement in circumferential direction (see Fig. 1)
w	out-of-plane displacement, positive inwards (see Fig. 1)
w'	dimensionless out-of-plane displacement, $w' = w/t$
x	meridional coordinate measured from the small radius, $0 \leqslant x \leqslant L$ (see Fig. 1)
y	circumferential curvilinear coordinate, $0 \leqslant y \leqslant 2\pi R_1$ (see Fig. 1)
Z	Batdorf parameter
α	tapering angle of cone
β_m	dimensionless meridional buckling wavenumber for cylinders (see Eq. (11a))
$\bar{\beta}_m$	dimensionless meridional buckling wavenumber for cones (see Eq. (24a))
β_c	dimensionless circumferential buckling wavenumber for cylinders (see Eq. (11b))
$\bar{\beta}_c$	dimensionless circumferential buckling wavenumber for cones (see Eq. (24b))
γ	dimensionless geometric parameter of cone (see Eq. (21))
ϑ	circumferential coordinate, $0 \leqslant \vartheta \leqslant 2\pi$ (see Fig. 1)
ϑ'	modified circumferential coordinate, $\vartheta' = \vartheta \sin\alpha$
ϑ_0	angular width of the finite element panel model (see Fig. 3)
λ	linear meridional bending half wavelength for cylinders (see Eq. (7))
$\bar{\lambda}$	average linear meridional bending half wavelength for cones (see Eq. (26))
ν	Poisson's ratio
$\rho(x)$	radius of curvature of cone at any point, $\rho(x) = R(x)/\cos\alpha$ (see Fig. 1)
$\bar{\rho}$	average radius of curvature of cone, $\bar{\rho} = (\rho_1 + \rho_2)/2$

φ	stress function
φ'	dimensionless stress function (see Eq. (21))
∇^4	fourth-order partial differential operator (see Eq. (4))
$\overline{\nabla}^2$	second-order partial differential operator (see Eq. (22))

Subscripts

1	referring to small-radius end
2	referring to large-radius end

imperfection sensitivity. Together with cylinders, cones or truncated cones (frusta) are the other single-curvature shells of revolution. Nevertheless, the buckling of axially compressed conical shells has attracted much more limited attention in comparison to their cylindrical counterparts.

Classical buckling analysis of cylinders under axial compression is based on the hypotheses of membrane prebuckling state, i.e. prebuckling rotations due to Poisson's effect along the curved edges are neglected (hence, such an analysis is referred to as for infinite shell length), and of shallow shell theory of Donnell (1934), Mushtari (1938) and Vlasov (1949), (see also the kinetic relationships of Sanders (1963) and Koiter (1966)). Based on the above hypotheses the critical buckling load, obtained for an axisymmetric mode by Lorenz (1908), Timoshenko (1910) and Southwell (1914), is

$$P_{\mathrm{cyl}} = \frac{2\pi E t^2}{\sqrt{3(1-\nu^2)}} \tag{1}$$

The axisymmetric buckling mode is described by a sine function with a constant amplitude. Donnell (1934) obtained the same critical load for asymmetric buckling modes, which are characterised by sine functions with different combinations of meridional and circumferential numbers of waves. As has been shown by Koiter (1945), the pairs of the meridional and circumferential buckling waves are distributed along a circle in a dimensionless wavenumber space. Such a locus is commonly known as the *Koiter circle* (see Calladine, 1983, Section 14.3, for a modern account).

As is mentioned above, the critical buckling load obtained from linear eigenvalue analysis might not give us exhaustive information regarding the actual collapse load of shells. For this purpose, the so-called postbuckling behaviour has to be analysed without limitations on the entity of displacements (large displacement non-linear analysis). Non-linear analyses were carried out for axially compressed cylinders by von Karman and coworkers (von Karman et al., 1940; von Karman and Tsien, 1941) and, independently, by Cicala (1944). In von Karman et al. (1940), a rigid-bar model with a non-linear spring was examined and a simple physical explanation of the strong postbuckling load drop and imperfection sensitivity was presented.

The asymptotic analysis of Koiter (1945) supplied a sound basis for studying postbuckling behaviour. Accordingly, it is assumed that, in the initial postbuckling stage, the deformed shape is that of the buckling mode, and as such the first and second derivatives of the total potential energy with respect to a scalar variable amplifying the buckling mode allow us to determine the equilibrium paths and their stability conditions, respectively. When simultaneous or nearly simultaneous buckling modes occur, there is a 'competing' interaction between modes so that severely unstable paths coupling more than one mode generate (see e.g. Bazant and Cedolin, 1991, Section 7.7; and Gioncu, 1994 for a general account). The simple Augusti's model elucidates this phenomenon (Augusti, 1964). An account of the problem of mode interactions along with its imperfection sensitivity implications in shells structures (specifically axially compressed cylindrical shells) is given in Hutchinson and Koiter (1970).

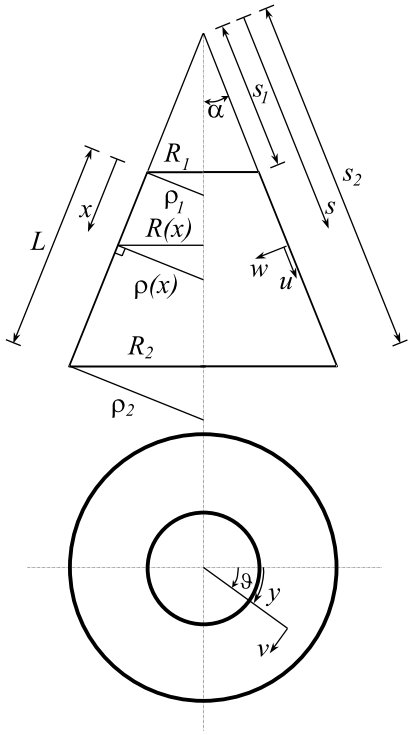

Fig. 1. Coordinates and nomenclature of the conical shell.

Conical shells exhibit a buckling behaviour which is somehow similar to that illustrated before for cylinders. In particular, there are evidences that also conical shells subject to axial compression are imperfection sensitive (Lackman and Penzien, 1960; Spagnoli, 1994; Chryssanthopoulos et al., 1997; Spagnoli, 2001). The classical buckling analysis of axially compressed cones is based on the same hypotheses exploited for cylindrical shells (membrane prebuckling state and shallow shell theory of Donnell–Mushtari–Vlasov). Seide (1956) firstly derived the critical buckling load for an axisymmetric mode, solving the determinant of stability equations for Poisson's ratio equal to zero. Such a load is given by the following simple expression

$$P_{\text{cone}} = \frac{2\pi E t^2}{\sqrt{3(1-\nu^2)}} \cos^2 \alpha = P_{\text{cyl}} \cos^2 \alpha \tag{2}$$

Seide's solution considers an axisymmetric mode, where the out-of-plane displacement w (see Fig. 1) is given as a linear combination of Bessel functions of the first and second kinds. Lackman and Penzien (1960) demonstrated that Seide's critical load is also applicable to non-zero values of the Poisson's ratio.

Singer (1965), using the asymmetric buckling mode shapes introduced by the same author in a preceding publication (sine functions with an exponential amplitude, see Eq. (17) of Singer (1961)) and the Galerkin method, obtained the same Seide's buckling load. In 1970, two independent papers by Baruch et al. and Tani and Yamaki also calculated buckling loads for asymmetric modes using the Galerkin method. The adopted buckling mode shapes are described again by sine functions with an exponential amplitude (see Eq. (3) of Baruch et al., 1970 , and Eq. (9) of Tani and Yamaki, 1970). However, none of the above papers related to asymmetric buckling of axially compressed cones indicated the existence of simultaneous modes.

An attempt to explore the presence of simultaneous buckling modes in cones has been presented by Poggi (1989). More recently, Pariatmono and Chryssanthopoulos (1995) extensively compared the previous solutions of Baruch et al. (1970) and Tani and Yamaki (1970), showing that, in certain cases, different buckling modes correspond to the same value of critical load.

In the present paper, the problem of simultaneous buckling modes in axially compressed conical shells is thoroughly analysed via linear eigenvalue analysis. Finite element (FE) models of a conical panel with symmetry/antisymmetry boundary conditions along the two meridians are employed. By varying the angular width of the panel, the number of circumferential buckling waves is enforced, allowing a mapping of the simultaneous doubly periodic buckling modes. The locus of numbers of meridional and circumferential buckling waves for simultaneous modes is described by an ellipse (hereafter termed as the *Koiter ellipse*) in a specifically defined dimensionless wavenumber space. The aspect ratio of such an ellipse is a function of the tapering angle α, and approaches the limit case of the Koiter circle for cylinders as α tends to zero.

2. Classical buckling analysis of cylindrical shells

2.1. Governing equation and axisymmetric buckling mode

The governing stability equation of Donnell for axially compressed cylinders can be written as follows (see, for instance, Brush and Almroth, 1975 , Section 5.5b):

$$D\nabla^4(\nabla^4 w) + \frac{1-\nu^2}{R^2} C w_{,xxxx} + \frac{P}{2\pi R}\nabla^4 w_{,xx} = 0 \tag{3}$$

where w is the incremental out-of-plane displacement with respect to the initial (prebuckling) state, the comma subscript corresponds to partial differentiation against the variable indicated, and

$$\nabla^4(\ ) = (\ )_{,xxxx} + \frac{2}{R^2}(\ )_{,xx\vartheta\vartheta} + \frac{1}{R^4}(\ )_{,\vartheta\vartheta\vartheta\vartheta} \tag{4}$$

The coordinates x and ϑ are reported in Fig. 1 (for $\alpha = 0°$).

The solution of Eq. (3) is given by the following axisymmetric buckling mode (eigenvalue), (e.g. see Timoshenko, 1910):

$$w(x) = \sin\left(\frac{\pi x}{l_m}\right) \tag{5}$$

where $l_m = L/m$ is the meridional buckling half wavelength. The corresponding buckling load (eigenvector) is equal to:

$$P = \frac{2\pi E t^2}{\sqrt{3(1-\nu^2)}}\left[\left(\frac{l_m}{\lambda}\right)^2 + \frac{1}{4}\left(\frac{\lambda}{l_m}\right)^2\right] \tag{6}$$

where λ is the half wavelength according to the linear bending theory for cylinders, i.e.

$$\lambda = \frac{\pi}{\sqrt[4]{3(1-\nu^2)}}\sqrt{Rt} \tag{7}$$

The length λ corresponds to the difference between two successive values of the meridional coordinate at which the meridional moment is equal to zero.

The critical buckling load for the axisymmetric mode is given by Eq. (1), and is obtained by minimizing Eq. (6) against the number of meridional buckling half waves. The minimizing meridional half wavelength is equal to

$$l_0 = \frac{\lambda}{\sqrt{2}} = \frac{\pi}{\sqrt[4]{12(1-\nu^2)}}\sqrt{Rt} \tag{8}$$

2.2. Doubly periodic buckling modes and the Koiter circle

The solution of Eq. (3) for asymmetric buckling modes (eigenvectors) is given by the following doubly periodic function (Donnell, 1934):

$$w(x,y) = \sin\left(\frac{\pi x}{l_\mathrm{m}}\right)\sin\left(\frac{\pi y}{l_\mathrm{c}}\right) \tag{9}$$

where l_m and l_c are the meridional and circumferential buckling half wavelength, respectively

$$l_\mathrm{m} = \frac{L}{m} \tag{10a}$$

$$l_\mathrm{c} = \frac{\pi R}{n} \tag{10b}$$

By introducing the following dimensionless wavenumbers

$$\beta_\mathrm{m} = \frac{\lambda}{l_\mathrm{m}} \tag{11a}$$

$$\beta_\mathrm{c} = \frac{\lambda}{l_\mathrm{c}} \tag{11b}$$

the buckling load (eigenvalue) corresponding to the solution (9) of Eq. (3) can be written as

$$P = \frac{2\pi E t^2}{\sqrt{3(1-\nu^2)}}\left(A + \frac{1}{4A}\right) = P_\mathrm{cyl}F(\beta_\mathrm{m},\beta_\mathrm{c}) \tag{12}$$

where

$$A = \frac{\beta_\mathrm{m}^2}{(\beta_\mathrm{m}^2+\beta_\mathrm{c}^2)^2} \tag{13}$$

As is shown in Fig. 2, the locus of the constant A in the dimensionless wavenumber space β_m–β_c is described by the equation of a circle (the *Koiter circle*):

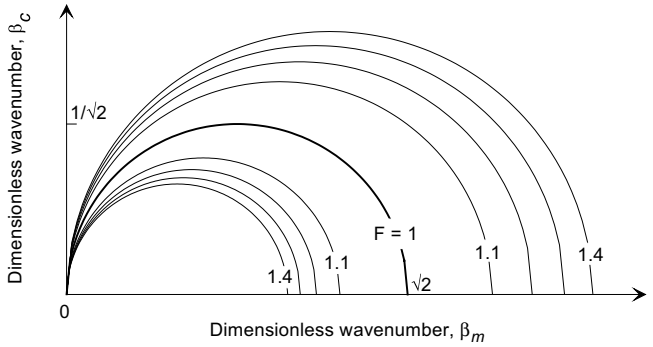

Fig. 2. Koiter circles for axially compressed cylindrical shells in the β_m–β_c dimensionless wavenumber space.

$$\frac{(\beta_m - a)^2}{a^2} + \frac{\beta_c^2}{a^2} = 1 \tag{14}$$

where the radius a of the circle is equal to:

$$a = \sqrt{A} \tag{15}$$

The minimum of Eq. (12) ($P = P_{cyl}$) is for $F = 1$, i.e. for $A = 1/2$. The corresponding radius of the Koiter circle becomes

$$a = \sqrt{A} = \frac{1}{\sqrt{2}} = \frac{\beta_0}{2} \tag{16}$$

where

$$\beta_0 = \frac{\lambda}{l_0} \tag{17}$$

The above-reported buckling load and modes obtained from the solution of Donnell stability equation refer to simply supported (SS) boundary conditions along the curved edges of the cylinder ($w = 0$ and $w_{,xx} = 0$ at $x = 0, L$). Boundary conditions on the displacements u and v are ignored.

2.3. Effect of the shell finite length

Since both m and n are positive integers for cylinders of finite length, only discrete values of β_m and β_c should be considered in Eq. (14). The spacing of the discrete values of β_m and β_c can be obtained from Eqs. (7), (10) and (11), i.e.

$$\Delta\beta_m = \frac{\lambda}{L} = \frac{\pi}{\sqrt[4]{3(1-\nu^2)}} \frac{\sqrt{Rt}}{L} \tag{18a}$$

$$\Delta\beta_c = \frac{\lambda}{\pi R} = \frac{1}{\sqrt[4]{3(1-\nu^2)}} \sqrt{\frac{t}{R}} \tag{18b}$$

Note that the discrete values of β_m and β_c lie at the nodal points of a rectangular grid (see Fig. 4), and that the aspect ratio of the unit cell of the grid is equal to $L/\pi R$ (see Fig. 14.8 of Calladine, 1983). Thus, the pairs of meridional and circumferential buckling wavenumbers do not exactly fall on the Koiter circle. However, given the small values of $\Delta\beta_m$ and $\Delta\beta_c$ for typical dimensions of cylindrical shell structures in comparison to the radius a of the Koiter circle, P is nearly equal to P_{cyl} for many pairs of m and n values (see Fig. 14.9 of Calladine, 1983).

The minimization of Eq. (12) leading to the critical load P_{cyl} is performed considering m as a continuously variable. As is mentioned above, for shells of finite length, m is an integer, and as such P calculated from Eq. (12) might result to be higher than P_{cyl}. The minimum value of L (being $m = 1$) for which $P = P_{cyl}$ defines the lower limit of the range of applicability of Eq. (12) (called range of moderately long cylinders), that is:

$$L \geqslant 1.69 \frac{\sqrt{Rt}}{\sqrt[4]{(1-\nu^2)}} \tag{19}$$

The above inequality corresponds to a value of the Batdorf parameter Z higher that 2.85 (Batdorf, 1947). Obviously, the upper limit of applicability of the Donnell formulation is given by the buckling of the cylinder as a column with undeformed cross-sections ($m = n = 1$), (called range of very long cylinders).

3. Buckling analysis of conical shells

3.1. Classical theory and governing equations

The governing stability equations of Donnell for axially compressed cones can be written in the following $\varphi - w$ coupled form, where φ is a stress function and w is the incremental out-of-plane displacement with respect to the initial (prebuckling) state (see, for instance, Pariatmono and Chryssanthopoulos, 1995):

$$\begin{aligned} &\overline{\nabla}^2(\overline{\nabla}^2\varphi') = -\frac{1}{s'}w'_{,s's'} \\ &\overline{\nabla}^2(\overline{\nabla}^2 w') + P'\frac{1}{s'}w'_{,s's'} - 12\gamma^2\frac{1}{s'}\varphi'_{,s's'} = 0 \end{aligned} \tag{20}$$

where the following dimensionless quantities are used:

$$\begin{aligned} \varphi' &= \frac{\varphi}{Et^2 s_2 \cot\alpha} \\ P' &= 4\frac{P}{P_{\text{cone}}}\sqrt{3(1-\nu^2)}\frac{s_2}{t}\cot\alpha \\ \gamma &= \frac{s_2^2}{R_2 t}\cos\alpha\sqrt{1-\nu^2} \end{aligned} \tag{21}$$

along with the second-order partial differential operator:

$$\overline{\nabla}^2(\ ) = (\ )_{,s's'} + \frac{1}{s'}(\ )_{,s'} + \frac{1}{s'^2}(\ )_{,\vartheta'\vartheta'} \tag{22}$$

As is presented in Section 1, no closed-form solutions of Eq. (20) for asymmetric buckling modes of axially compressed conical shells are available in the literature, being the existing solutions (Singer, 1965; Baruch et al., 1970; Tani and Yamaki, 1970) based on the Galerkin method.

It is worth recalling that in the buckling analysis of conical shells, conversely to cylindrical shells, the application of translational constraints along the curved edges is twofold. Simple supports can be defined in fact by either the condition of $u\sin\alpha - w\cos\alpha = 0$ and $v = 0$ (hereafter called 'ring' boundary conditions) representing the actual constraint imposed by bulkheads that are rigid in a plane perpendicular to the cone axis, or the condition of $w = 0$ and $v = 0$ (hereafter called 'cylinder' boundary conditions) representing zero out-of-plane displacements along the curved edges. Note that Seide (1956) along with Lackman and Penzien (1960) considered SS 'ring' boundary conditions, while the other authors cited in Section 1 analysed different 'cylinder' boundary conditions (Table 1). In particular, Baruch et al. (1970) studied SS boundary conditions, while Tani and Yamaki (1970) and Pariatmono and Chryssanthopoulos (1995) considered both SS and clamped (CC) boundary conditions.

3.2. Linear-eigenvalue analysis and finite element modelling

A linear eigenvalue FE analysis using the general-purpose computer program ABAQUS (Hibbit et al., 2002) is carried out to determine the elastic critical buckling load and the corresponding modes of axially compressed conical shells with different values of the tapering angle. The use of the FE method for solving such a linear stability problem is supported by the fact that general buckling mode shapes can be described. FE models of a portion of the conical shell limited by two meridians (panel model) are built up along with axisymmetric models. For the panel model, nine-node Lagrange shell elements (ABAQUS element type S9R5), based on the degenerated shell theory and Mindlin kinematic assumptions, are employed. The above FE uses a reduced 2×2 Gauss integration and has five degrees of freedom per node. The element

Table 1
Translational out-of-plane end-constraints in previous theoretical studies, and applied boundary conditions along the curved and meridional edges in the present FE panel model, during prebuckling stage and at buckling

	Theory		Present FE model	
	'Ring' b.c.[a]	'Cylinder' b.c.[b]	Curved edges[c]	Meridional edges
Prebuckling	–	–	$v = 0$ $u\sin\alpha - w\cos\alpha = 0$	Sym[d]+Sym[d]
Buckling	$u\sin\alpha - w\cos\alpha = 0$	$w = 0$	$v = 0$	Sym[d]+Asym[e]

[a] See Lackman and Penzien (1960) and Seide (1956).
[b] See Baruch et al. (1970), Tani and Yamaki (1970) and Pariatmono and Chryssanthopoulos (1995).
[c] u = constant along the small-radius end and $u = 0$ along the large-radius end.
[d] Symmetry boundary conditions: $v = \varphi_u = \varphi_w = 0$ (φ_u = rotation about u—direction, φ_w = rotation about w—direction).
[e] Antisymmetry boundary conditions: $u = w = \varphi_v = 0$ (φ_v = rotation about v—direction).

formulation is based on a large displacement and small strain analysis. For axisymmetric models, a 3-node axisymmetric element (ABAQUS element type SAX2) is adopted. The value of the Poisson's ratio v is kept equal to 0.3.

Radially fixed rotationally free SS 'ring' boundary conditions ($u\sin\alpha - w\cos\alpha = 0$ and $v = 0$) are applied along the curved edges (ends) of the panel model (axisymmetric model). The models are loaded by imposing uniform meridional displacements along the small radius end (u = constant), and by constraining the corresponding displacements along the large radius end ($u = 0$). Symmetry and antisymmetry boundary conditions along the two meridians, respectively, of the panel model are adopted, which allows us to model a quarter of circumferential buckling wave. In the formation of the conventional stiffness matrix (prebuckling stage) membrane boundary conditions ($u = 0$ and $v = 0$) and symmetry boundary conditions are applied along the curved edges and the two meridians, respectively. The adopted boundary conditions in the panel model are summarised in Table 1.

By varying the panel width of the FE model, the number of circumferential buckling waves can be enforced (Fig. 3). Being ϑ_0 the panel angular width, the following number of circumferential buckling waves is imposed (provided that a quarter of circumferential wave develops within the panel):

$$n = \frac{\pi}{2\vartheta_0} \tag{23}$$

For axisymmetric FE models, axisymmetric buckling modes ($n = 0$) are picked up.

Convergence studies have been undertaken to ensure that the adopted meshes produce accurate results for buckling load and mode predictions. For panel models, the adopted mesh presents a maximum angular

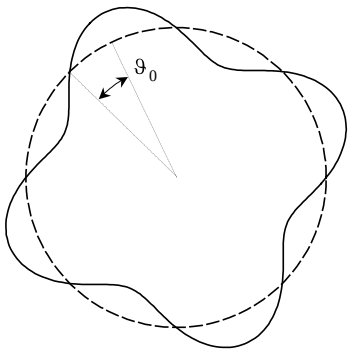

Fig. 3. Angular width of the FE panel model (e.g. $\vartheta_0 = 22.5°$) and circumferential profile of the related buckling mode (e.g. $n = 4$).

width for each element equal to 1.5°. The meridional number of elements is determined so that each element has an aspect ratio approximately equal to unity near the small-radius end (near the large-radius end the aspect ratio attains the maximum value of 3.7 for $\alpha = 60°$). The following values of the geometric parameters are kept constant while varying the tapering angle α ($\alpha = 0°$, 15°, 30°, 45° and 60°): $t = 1$ mm, $R_1/t = 1000$, $L/R_1 = 3$. The value of the ratio L/R_1 has been chosen in order to obtain an approximately square grid of discrete values in the β_m–β_c space ($L/\pi R_1 \approx 1$, see Section 2.3). The maximum value of tapering angle considered is linked to the limit value commonly adopted in the buckling analysis and design of conical shells (e.g. see ECCS, 1988). Beyond such a value, aspects related to snap-through instability might be more relevant than those, here investigated, related to bifurcation instability. For panel models, the analyses are performed with an angular width ϑ_0 varying from 2.8° to 45° (according to Eq. (23), n ranges from 32 to 2). A total number of 155 analyses are performed, and 20 eigenvalues/eigenvectors are extracted for each analysis.

Doubly periodic buckling modes (see Eq. (9)) are obtained from FE analyses of panel models. The number of circumferential buckling waves n is determined from Eq. (23) when a quarter of circumferential wave develops within the panel. Wide panels (having ϑ_0 higher than 11.25°) exhibit occasionally a 3/4-circumferential wave, and the number n is calculated accordingly. A few modes (less than 5% of the total eigenmodes extracted), given by the superposition of a certain asymmetric mode with an axisymmetric barrel model (having a single half-wave in the meridional direction), are detected. Also, a number of modes (about 11% of the total eigenmodes extracted), given by the superposition of two asymmetric modes with the same number n of circumferential waves, are observed. In the former cases, the pair of meridional and circumferential waves of the mode superimposing the barrel one is counted (and reported in the wavenumber spaces of Figs. 4 and 5, see Section 3.3), while in the latter cases, the two pairs of meridional and circumferential waves of the combined modes are considered (n is the same for both the modes). In a few cases (for $\alpha \neq 0°$), a small decay in the amplitude of the buckling mode in the meridional direction, from the small- to the large-radius end, is experienced. However, since in the present study simultaneous buckling modes are analysed only in terms of wavenumbers, decaying modes are also reported in the wavenumber spaces of Figs. 4 and 5 (see Section 3.3) by neglecting their varying amplitude. Some spurious modes, representing less than 2% of the total eigenmodes extracted, are detected. Such modes are not considered in the discussion of Section 3.3 since they are connected to numerical instabilities and, hence, they are not realistic. It is seen that the frequency of occurrence of either spurious or non-constant amplitude modes (barrel modes, superimposed modes and decaying modes) does not increase with increasing tapering angle. Moreover, no clear tendency in the distribution of the corresponding buckling loads is observed.

3.3. Locus of simultaneous buckling modes

Now let us consider, for each value of the tapering angle α, the simultaneous buckling modes obtained from FE analyses. By taking the buckling modes related to $P \leqslant 1.02P_{cone}$ (including also axisymmetric modes, $n = 0$) and plotting the pairs of meridional and circumferential wavenumbers in the β_m–β_c space, a comparison with the Koiter circle for cylinders (see Eq. (14)) is made (Fig. 4). For the sake of completeness, the grid in the β_m–β_c space with spacing defined by Eq. (18) is also plotted in Fig. 4. It can be observed that there is a deviation of the locus of simultaneous buckling modes for cones from that described by the Koiter circle. In particular, the number of meridional buckling half waves for cones is smaller than that of a cylinder having height and radius equal to the slant length and minimum radius of the examined cone, respectively (in the present study, the ratios L/R_1 and R_1/t are kept constant while α varies).

Since the radius of curvature ρ of cones is a function of the meridional coordinate x (Fig. 1), it is here proposed to use a new normalisation for the buckling wavenumber space, which is based on the average values of the geometric parameters of the cone, i.e.

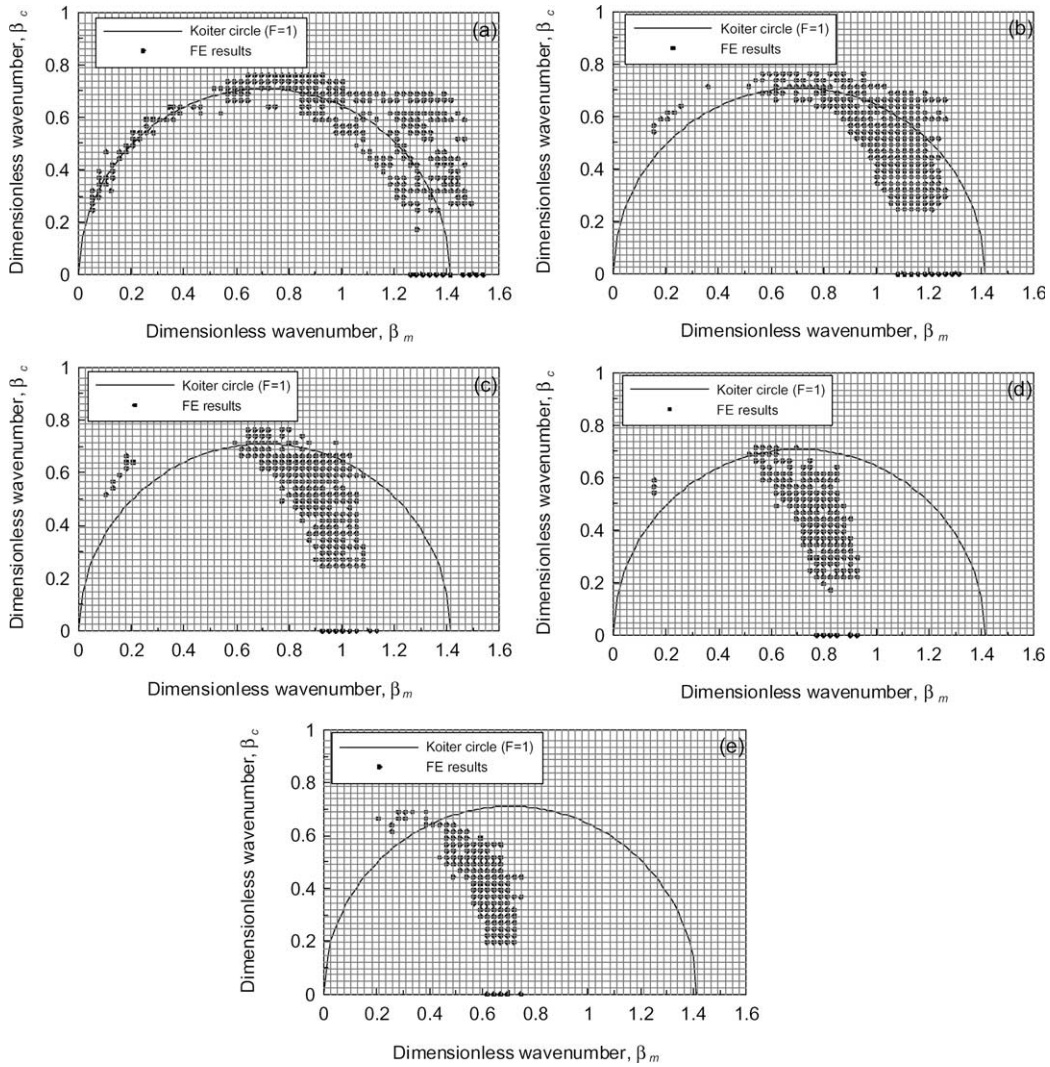

Fig. 4. Koiter circle ($F = 1$) for cylinders and FE buckling modes with $P \leqslant 1.02P_{\text{cone}}$ for cones in the β_{m}–β_{c} dimensionless wavenumber space: (a) cylinder ($\alpha = 0°$), (b) $\alpha = 15°$, (c) $\alpha = 30°$, (d) $\alpha = 45°$ and (e) $\alpha = 60°$.

$$\bar{\beta}_{\text{m}} = \frac{\bar{\lambda}}{\bar{l}_{\text{m}}} \tag{24a}$$

$$\bar{\beta}_{\text{c}} = \frac{\bar{\lambda}}{\bar{l}_{\text{c}}} \tag{24b}$$

where

$$\bar{l}_{\text{m}} = l_{\text{m}} = \frac{L}{m} \tag{25a}$$

$$\bar{l}_{\text{c}} = \frac{\pi\bar{\rho}}{n} \tag{25b}$$

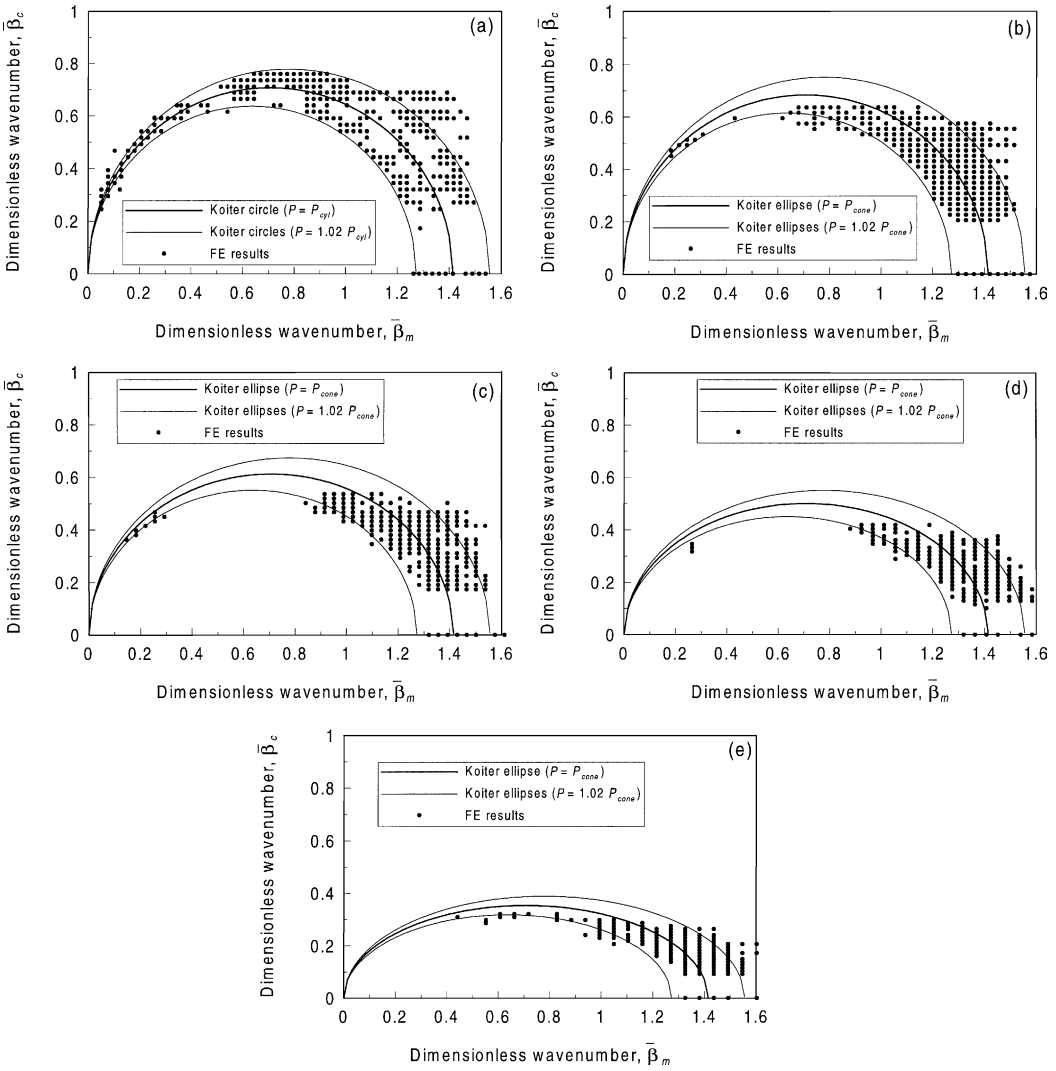

Fig. 5. Locus of simultaneous buckling modes (Koiter ellipses for $P = P_{\text{cone}}$ and $P = 1.02P_{\text{cone}}$) and FE buckling modes with $P \leqslant 1.02P_{\text{cone}}$ for cones in the $\bar{\beta}_{\text{m}}$–$\bar{\beta}_{\text{c}}$ dimensionless wavenumber space: (a) cylinder ($\alpha = 0°$), (b) $\alpha = 15°$, (c) $\alpha = 30°$, (d) $\alpha = 45°$ and (e) $\alpha = 60°$.

and

$$\bar{\lambda} = \frac{\pi}{\sqrt[4]{3(1-\nu^2)}}\sqrt{\bar{\rho}t} \tag{26}$$

The value $\bar{\lambda}$ of Eq. (26), based on the average radius of curvature $\bar{\rho}$, corresponds to the average half wavelength according to the linear bending theory for cones. In fact, it has been verified through linear elastic analysis of an axisymmetric FE model that, at the two ends of the cone, the wavelength λ is dependent on the local radius of curvature (λ is proportional to $\sqrt{\rho_1}$ and $\sqrt{\rho_2}$, at the small- and large-radius end, respectively).

The same FE modes reported in Fig. 4 (related to $P \leqslant 1.02P_{\text{cone}}$) are presented in Fig. 5 according to the proposed normalisation of the wavenumber space ($\bar{\beta}_{\text{m}}$–$\bar{\beta}_{\text{c}}$ space). It can be seen that the locus of simultaneous buckling modes can now be described by an ellipse (called the *Koiter ellipse*), namely

$$\frac{(\bar{\beta}_{\text{m}} - \bar{a})^2}{\bar{a}^2} + \frac{\bar{\beta}_{\text{c}}^2}{\bar{b}^2} = 1 \tag{27}$$

where

$$\bar{a} = \frac{1}{\sqrt{2}} \tag{28a}$$

$$\bar{b} = \frac{\cos\alpha}{\sqrt{2}} \tag{28b}$$

This is supported by the fact that many FE buckling wavenumbers fall in the region enclosed by the Koiter ellipses for $P = 1.02P_{\text{cone}}$. In line with Eqs (12) and (15) for cylinders, such ellipses are assumed to have semiaxes equal to 1.1 and 0.9 times the values of $\bar{a}$ and $\bar{b}$ of Eq. (28) (according to Eq. (12), for $F = 1.02\,A$ is equal to 0.610 and 0.410, and from Eq. (15) $a = 0.781$ and 0.640, respectively, that is, $0.781 \approx 1.1/\sqrt{2}$ and $0.640 \approx 0.9/\sqrt{2}$).

Note that the value of $P = 1.02P_{\text{cone}}$ has arbitrarily been chosen in order to have a relatively large number of discerete values in the β_{m}–β_{c} space (see nodal-points of the grid reported in Fig. 4) falling in the half crescent-like region enclosed by the Koiter ellipses for $P = 1.02P_{\text{cone}}$. In fact, owing to the finite length of the conical shell analysed ($t = 1$ mm, $R_1/t = 1000$, $L/R_1 = 3$), the values of β_{m} and β_{c} (as well as those of $\bar{\beta}_{\text{m}}$ and $\bar{\beta}_{\text{c}}$) for the extracted FE buckling modes (with $P \leqslant 1.02P_{\text{cone}}$) lay on the nodal-points mentioned above.

In Fig. 6, the variation of the locus of simultaneous buckling modes in the $\bar{\beta}_{\text{m}}$–$\bar{\beta}_{\text{c}}$ space is presented as a function of the tapering angle α. It can be noted that, while the shape of such a locus changes from a circle for cylinders ($\alpha = 0°$) to ellipses for cones (with $\bar{b} = \bar{a}\cos\alpha$), the dimensionless meridional wavenumber $\bar{\beta}_0$ for axisymmetric buckling remains constant ($\bar{\beta}_0 = \sqrt{2}$). This implies that the corresponding meridional buckling half wavelength l_0 is equal to $\bar{\lambda}/\sqrt{2}$ (see Eq. (17) for $\lambda = \bar{\lambda}$) for any value of the tapering angle α, being the effect of α incorporated in the new definition of the wavelength $\bar{\lambda}$ (Eq. (26)). Moreover, it is worth recalling that, following the proposed normalisation of the buckling wavenumber space, the distribution of simultaneous buckling modes for cones can be seen as that of an equivalent cylinder of equal thickness with

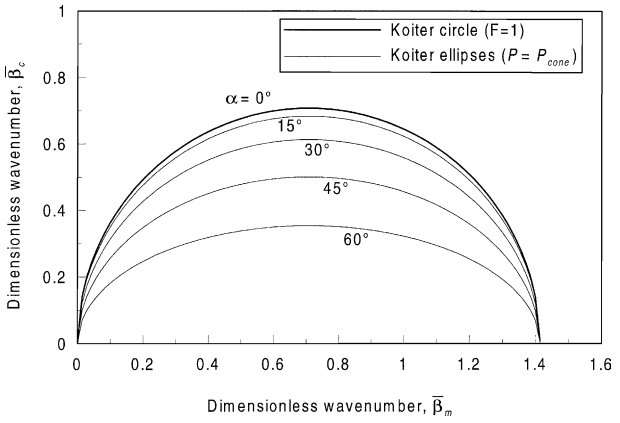

Fig. 6. Locus of simultaneous buckling modes (Koiter ellipses for $P = P_{\text{cone}}$) in the $\bar{\beta}_{\text{m}}$–$\bar{\beta}_{\text{c}}$ dimensionless wavenumber space for different values of the tapering angle α.

radius $\bar{\rho}$ and height L. As is stated above, the tapering angle α plays a role only in affecting the ratio $\bar{b}/\bar{a}$ between semiaxes (Eqs. 28a,28b) of the Koiter ellipses ($\bar{b}/\bar{a} = 1$ for cylinders, that is, the Koiter circle).

Finally, it should be mentioned that, if $\bar{l}_c$ is assumed to be equal to $\pi\overline{R}/n$ (this might be more appropriate from a geometrical point of view, since the average length of the parallels of the cone along which circumferential buckling waves develop is equal to $2\pi\overline{R}$) instead of using the definition (25b), the locus of dimensionless wavenumbers for simultaneous buckling modes can be described by the Koiter circle for any value of α. However, the definition (25b) is deemed to be preferable since it relates the buckling behaviour of conical shells to that of their cylindrical counterparts, and as such the present study can be placed in the main stream of equivalent cylinder approaches commonly used in the approximate methods of buckling analysis and design of cones (e.g. see Finzi and Poggi, 1987 and ECCS, 1988).

4. Conclusions

The salient points of the present study include:

(i) Linear eigenvalue analysis of FE models (panel model and axisymmetric model) provides evidence of the existence of simultaneous buckling modes for conical shells under axial compression;
(ii) The number of meridional buckling half waves for cones is smaller than that of a cylinder of equal thickness having height and radius equal to the slant length and minimum radius of cone, respectively;
(iii) The pairs of circumferential and meridional buckling waves for a conical shell corresponding to the same critical load tend to describe, in a specifically defined dimensionless wavenumber space, an ellipse (here termed as the Koiter ellipse) whose aspect ratio is equal to $\cos\alpha$, where α is the tapering angle of cone;
(iv) The distribution of simultaneous buckling modes for cones can be seen as that of an equivalent cylinder of equal thickness with radius $\bar{\rho}$ and height L. The tapering angle α plays a role only in affecting the ratio $\bar{b}/\bar{a}$ between the semiaxes of the Koiter ellipses ($\bar{b}/\bar{a} = 1$ for cylinders, that is, the Koiter circle).

In conclusion, the present paper, by providing evidence of the existence of simultaneous buckling modes, might offer a starting point from which the imperfection sensitivity of cones, particularly in terms of juxtaposing cones to cylinders, can then be investigated (e.g. through non-linear analysis of FE models with eigenmode-affine imperfections).

References

Augusti, G., 1964. Stabilità di strutture elastiche elementari in presenza di grandi spostamenti. In: Atti della Accademia Nazionale dei Lincei di Scienze Fisiche-Matematiche e Naturali, vol. 4, no. 5, Series 3 (in Italian).

Baruch, M., Harari, O., Singer, J., 1970. Low buckling loads of axially compressed conical shells. J. Appl. Mech. Trans. ASME 37, 384–392.

Batdorf, S.B., 1947. A simplified method of elastic stability analysis for thin cylindrical shells. NACA Report 874.

Bazant, Z.P., Cedolin, L., 1991. Stability of Structures. Oxford University Press, Oxford.

Brush, D.O., Almroth, B.O., 1975. Buckling of Bars, Plates, and Shells. McGraw-Hill, New York.

Calladine, C.R., 1983. Theory of Shell Structures. Cambridge University Press, Cambridge.

Chryssanthopoulos, M.K., Pariatmono, N., Spagnoli, A., 1997. Buckling tests of unstiffened and stiffened conical shells in compression. In: Proceedings of the International Conference on Carrying Capacity of Steel Shell Structures, Brno, Czech Republic, pp. 16–23.

Cicala, A., 1944. Il cilindro in parete sottile compresso assialmente. Nuovo orientamento dell'indagine sulla stabilità elastica. L'Aerotecnica XXIV, 3–18 (in Italian).

Donnell, L.H., 1934. A new theory for the buckling of thin cylinders under axial compression and bending. J. Appl. Mech. Trans. ASME 56, 795–806.
ECCS TWG 8.4, 1988. Buckling of steel shells. European Convention for Constructional Steelwork.
Finzi, L., Poggi, C., 1987. Approximate formulas for the design of conical shells under various loading conditions. In: Proceedings of ECCS Colloquium on Stability of Plate and Shell Structures, Ghent University, pp. 397–404.
Gioncu, V., 1994. General theory of coupled instabilities. Thin-Walled Struct. 19, 81–127.
Hibbit, Karlsson, Soresen, 2002, ABAQUS Version 6.3 Standard User's Manual.
Hutchinson, J.W., Koiter, W.T., 1970. Post-buckling theory. Appl. Mech. Rev. 13, 1353–1366.
Koiter, W.T., 1945. Over de Stabiliteit van het Elastiche Evenwicht, Ph.D. Thesis, Delft University (in Dutch). (Translation: On the Stability of Elastic Equilibrium. AFFDL-TR-70-25, Wright-Patterson Air Force Base, 1970).
Koiter, W.T., 1966. On the nonlinear theory of thin elastic shells. Proc. K. Ned. Akad. Wet. Series B, 69.
Lackman, L., Penzien, J., 1960. Buckling of circular cones under axial compression. J. Appl. Mech. Trans. ASME 27 (3), 458–460.
Lorenz, R., 1908. Achsensymmetrische knickung dünnwandingen hohlzylindern (in German). Zeitschrift des Vereines Deutscher Ingenieure 52 (43), 1706–1713.
Mushtari, K.M., 1938. Some generalizations of the theory of thin shells with application to the stability problem of elastic equilibrium. Izv. Kaz. fiz-mat. o-va., Vol. XI, Series 3 (in Russian).
Pariatmono, N., Chryssanthopoulos, M.K., 1995. Asymmetric elastic buckling of axially compressed conical shells with various end-conditions. AIAA J. 33 (11), 2218–2227.
Poggi, C., 1989. On the Elastic-plastic Design of Unstiffened Conical Shells Subject to Axial Compression and External Pressure, DIC Thesis, Imperial College, London.
Sanders, J.L., 1963. Nonlinear theories for thin shells. Quart. Appl. Math. 21 (1), 21–36.
Seide, P., 1956. Axisymmetrical buckling of circular cones under axial compression. J. Appl. Mech. Trans. ASME 23 (4), 625–628.
Singer, J., 1961. Buckling of conical shells under axisymmetrical external pressure. J. Mech. Eng. Sci. 3 (4), 330–339.
Singer, J., 1965. Buckling of circular conical shells under uniform axial compression. AIAA J. 3 (5), 985–987.
Southwell, R.V., 1914. On the general theory of elastic stability. Phil. Trans. Royal Soc. London, Series A 213, 187.
Spagnoli, A., 1994. Buckling Behaviour and Design of Stiffened Conical Shells under Axially Compression, Ph.D. Thesis, Imperial College, University of London, 1997.
Spagnoli, A., 2001. Buckling modes in axially stiffened conical shells. Eng. Struct. 23 (8), 957–965.
Tani, J., Yamaki, N., 1970. Buckling of truncated conical shells under axial compression. AIAA J. 8 (3), 568–571.
Timoshenko, S.P., 1910. Einige stabilitätsprobleme der elastizitätstherie (in German). Zeitschrift für Angew. Math. Phys. (ZAMP) 58 (4), 337–385.
von Karman, T., Dunn, L.G., Tsien, H., 1940. The influence of curvature on the buckling characteristics of structures. J. Aeronaut. Sci. 7, 276–289.
von Karman, T., Tsien, H., 1941. The buckling of thin cylindrical shells under axial compression. J. Aeronaut. Sci. 8, 303–312.
Vlasov, V.Z., 1949. The General Theory of Shells and its Industrial Applications (in Russian). Gostekhizdat, Moscow.